

NJC

Accepted Manuscript



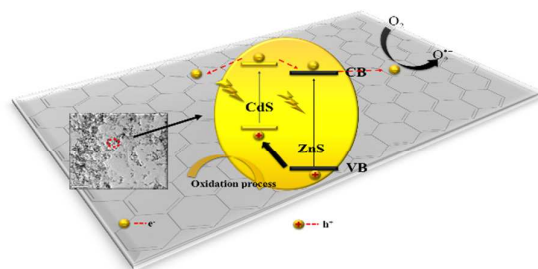
This is an *Accepted Manuscript*, which has been through the Royal Society of Chemistry peer review process and has been accepted for publication.

Accepted Manuscripts are published online shortly after acceptance, before technical editing, formatting and proof reading. Using this free service, authors can make their results available to the community, in citable form, before we publish the edited article. We will replace this *Accepted Manuscript* with the edited and formatted *Advance Article* as soon as it is available.

You can find more information about *Accepted Manuscripts* in the [Information for Authors](#).

Please note that technical editing may introduce minor changes to the text and/or graphics, which may alter content. The journal's standard [Terms & Conditions](#) and the [Ethical guidelines](#) still apply. In no event shall the Royal Society of Chemistry be held responsible for any errors or omissions in this *Accepted Manuscript* or any consequences arising from the use of any information it contains.

Graphical Abstract



The ternary RGO-CdS/ZnS heterostructures with an enhanced visible-light photocatalytic activity have been prepared by the facile hydrothermal method.

Enhanced photocatalytic degradation of tetracycline antibiotics by Reduced Graphene Oxide-CdS/ZnS heterostructure photocatalysts

Yanfeng Tang

School of Chemistry & Chemical Engineering, Jiangsu University, Zhenjiang 212013, People's Republic of China, Tel: +8613921599109 email: tangyanfenghnmz@gmail.com

Xinlin Liu

School of Materials Science & Engineering, Jiangsu University, Zhenjiang 212013, People's Republic of China, Tel: +8615050858583 email: xiaoliu1117@163.com

Changchang Ma

School of Chemistry & Chemical Engineering, Jiangsu University, Zhenjiang 212013, People's Republic of China, Tel: +8615050850448 email: machang719@163.com

Mingjun Zhou

School of Chemistry & Chemical Engineering, Jiangsu University, Zhenjiang 212013, People's Republic of China, Tel: +8615751011784 email: 15751011784@163.com

Pengwei Huo*

School of Chemistry & Chemical Engineering, Jiangsu University, Zhenjiang 212013, People's Republic of China, Tel: +8613511690255 email: tyfujs@126.com

Longbao Yu

School of Chemistry & Chemical Engineering, Jiangsu University, Zhenjiang 212013, People's Republic of China, Tel: +8618361811787 email: tangyanfenghnmz@foxmail.com

Jianming Pan

School of Chemistry & Chemical Engineering, Jiangsu University, Zhenjiang 212013, People's Republic of China, Tel: +8615952850631 email: pjn@ujs.edu.cn

Weidong Shi

School of Chemistry & Chemical Engineering, Jiangsu University, Zhenjiang 212013, People's Republic of China, Tel: +8615751011784 email: shiwd999@163.com

Yongsheng Yan*

School of Chemistry & Chemical Engineering, Jiangsu University, Zhenjiang 212013, People's Republic of China, Tel: +8615978753125 email: yys@mail.ujs.edu.cn

*Corresponding author: tyfujs@126.com (P. W. Huo) yys@mail.ujs.edu.cn (Y. Y. Yan)

Abstract In this work, Reduced Graphene oxide (RGO)-CdS/ZnS heterostructure composites have been successfully synthesized by the hydrothermal method with assembling the CdS/ZnS heterostructure nanoparticles on RGO sheets and the reduction of GO occurs simultaneously. The as-prepared RGO-CdS/ZnS composites with the content of 15% RGO exhibits highly active in photodegradation of TC. A possible mechanism for the enhanced photocatalytic activity has been discussed. The CdS/ZnS heterostructure facilitate the transformation of electrons which is excited by the light irradiation in the conduction band of CdS. RGO is supposed to be an electron transfer channel which is used to reduce the recombination of electron-hole pairs, thus enhancing the photo-conversion efficiency. By profiting from the synergy of RGO and CdS/ZnS heterostructure, the photocatalysts not only shows the better photocatalytic activity in tetracycline antibiotics but also prevents pure CdS or ZnS from photocorrosion. At last, RGO-CdS/ZnS shows the remarkable stability and cyclic performances.

Keywords: CdS/ZnS; Reduced Graphene Oxide; heterostructure; photocatalytic; tetracycline antibiotics

1. Introduction

Photocatalytic technology has attracted much attention due to its widely application in the degradation of waste water¹⁻³. Semiconductors photocatalysts, such as TiO₂⁴, WO₃^{5, 6}, ZnO⁷, have attracted great fundamental and technical research interest because of its high efficiency in degrading water contaminants without generating toxic by-products. Among various photocatalysts, cadmium sulfide (CdS) has been extensively studied due to the narrow band gap (2.4 eV) corresponding to the spectrum of visible-light, which makes it photo-excited easily under visible light irradiation. However, the low separation efficiency of electrons-hole pairs thus resulting in photocorrosion which prohibit the widely applications of CdS⁸. And also, the photocorrosion problem that the sulfide ion is highly prone to oxidation in photocatalytic activity, makes CdS very unstable and poor recyclable. To solve these problems, several approaches have been developed, such as synthesizing various structures (mesoporous⁹, nanoparticles¹⁰, nanowires¹¹), doping with elements^{12, 13}, hybridizing with polymers¹⁴, supporting with other materials¹⁵⁻¹⁸, coupling with other semiconductors^{19, 20}. Therefore, it is time to develop a highly efficient and robust visible-light responsive photocatalysts based on conventional semiconductor materials.

To date, more and more research has focused on CdS composites combined with other semiconductors which usually have significant advantages of promoting the separation of electron-hole pairs and keeping reduction and oxidation reactions at two different reaction sites^{21, 22}. Because of the narrow band gap of CdS, CdS-based

heterostructures have been extensively studied. Yin and co-workers have synthesized the core/sheath heterostructure CdS/TiO₂ nanotube arrays, which were prepared by electrochemically depositing CdS directly into anodic titanium nanotubes from an electrolyte containing Cd²⁺ and S²⁻ in dimethyl sulfoxide (DMSO), with enhanced solar water-splitting efficiency²³. The ZnO/CdS heterostructures have been synthesized by Xuewen Wang's group. Coupled ZnO/CdS heterostructures based on the Z-scheme mechanism are demonstrated to be highly active photocatalysts for H₂ evolution under simulated solar light irradiation due to the greatly prolonged lifetime of photoexcited carriers²⁴. Therefore, forming the CdS/ZnS heterostructure photocatalysts could be a promising method, because of ZnS which is an important II–VI semiconductor with a wide direct band gap and the same coordination mode with CdS. Also, it has been reported that combining CdS with other semiconductors (TiO₂, ZnO, etc.) or carbon based materials (carbon nanotube and graphene) can improve its photocatalytic activity^{16, 25, 26}. Among them, the preparation of individual graphene based on the CdS composite has been considered to be a promising method to overcome photocorrosion, since graphene is a chemically modified graphene owing to immense surface area of graphene (theoretically 2600 m²/g), chemical stability and high water solubility, good mechanical properties, and abundant sp²-hybridized 2D carbon network with extraordinary conductivity¹⁷. And RGO is supposed to be an electron transfer channel which is used to reduce the recombination of electron-hole pairs, thus enhancing photo-conversion efficiency of the photocatalytic materials, resulting in enhanced photo-conversion efficiency of the photocatalytic materials. Up

to now, there are several reports in the synthesis and application of graphene and CdS composites²⁷⁻²⁹. CdS clusters decorated graphene nanosheets have been prepared by Li et al. and exhibited higher hydrogen evolution rate than pure CdS nanoparticles²⁷. In addition, Cao et al. prepared graphene–CdS directly from GO in dimethyl sulfoxide (DMSO) through a facile one-step solvothermal method and exhibited higher hydrogen evolution rate than pure CdS nanoparticles²⁸. However in these works, only CdS nanoparticles were attached on the surface of RGO sheets. What's more, the previous report published is rarely focused on their photodegradation properties towards Tetracycline (TC) antibiotic. TC is a famous broad-spectrum antibacterial agent widely used for treating bacterial infection. Along with the worldwide application of TC antibiotic, the TC antibiotic residue which may pose threats and human health by inducing proliferation of bacterial drug resistance have reached a risk level in the environment³⁰. Considering the increasing potential threat for human health, tremendous efforts have been dedicated in water treatment researches to alleviate the deterioration of water body qualities around the world. However, the traditional treatments such as physical adsorption or chemical treatments couldn't remove antibiotic residue thoroughly from the environment. So, it is urgent for us to synthesize RGO–CdS/ZnS heterostructure composites with uniform deposition of CdS/ZnS heterostructure composites on RGO sheets and investigate the photocatalytic activity of RGO–CdS/ZnS composites.

Herein, RGO–CdS/ZnS heterostructure composites have been successfully synthesized by the facile hydrothermal method with assembling CdS/ZnS composites

on the surface of RGO sheets. RGO–CdS/ZnS composites take advantages of both components and acquire more benefits than previous CdS or ZnS involved photocatalysts, such as the uniform distribution of CdS/ZnS heterostructure composites on RGO sheets to facilitate charge transfer and reduce recombination rate of photo-generated electrons and holes, easy recovery of this composite due to the large size of RGO sheets, the excellent contact between CdS/ZnS composites and RGO sheets to prevent CdS from photocorrosion. In addition, RGO-CdS/ZnS composites show excellent photodegradation ability of Tetracycline antibiotic (TC) activity under visible light irradiation. The composites have exhibited great potential in water purification and disinfection fields.

2. Experimental section

2.1 Materials

Graphite powder, Sodium nitrate (NaNO_3 , 99%), Potassium permanganate (KMnO_4 , 99%), sulfuric acid (H_2SO_4 , 98%) and Hydrochloric acid (HCl , 37%) were obtained from Sinopharm Chemical Reagent Co. Ltd. Cadmium chloride hemi(pentahydrate) ($\text{CdCl}_2 \cdot 2.5\text{H}_2\text{O}$), Zinc chloride (ZnCl_2), Sodium sulfide ($\text{Na}_2\text{S} \cdot 9\text{H}_2\text{O}$), Hydrogen peroxide (H_2O_2 , 30%) were purchased from Aladdin Chemistry Co. Ltd. Tetracycline antibiotics were purchased from Shanghai Shunbo Biological Engineering Co. Ltd. In addition, all the materials used in the experimental were of analytical grade and directly used without any treatment. Furthermore, the water used in the experiment was doubly deionized water.

2.2 Catalyst preparation

2.2.1 Preparation of GO

GO was prepared using by the modified Hummer's method³¹. In briefly, graphite powder (1g) and 2.5g NaNO₃ was sequentially dispersed in a 250 mL round-bottom flask with cold concentrated sulphuric acid (30mL, 98wt.%, ice-bath) under magnetic stirring. Then potassium permanganate (KMnO₄, 4g) were slowly added into the mixture with continuous vigorous stirring and the ice bath which could prevent the temperature from exceeding 20 °C. The ice bath was removed and replaced by water bath after 2h stirring, then the mixture was heated to 35 °C for 30min, followed by slowly addition of deionized water (40 mL) which resulted in a rapid temperature increase (up to a maximum of 98 °C) in solution. In order to increase the oxidation degree of the GO product, the reaction was maintained for other 40 min. When the bright-yellow suspension was appearing, the mixture reaction was terminated by addition of more distilled water (140 mL), followed by a hydrogen peroxide solution (H₂O₂, 30%, 10 mL). The solid product was separated by filtration and washed with 200 mL of 1:10 HCl solution, and water until pH = 7. Finally, the powder was vacuum-dried at 60 °C for 24h.

2.2.2 Preparation of RGO-CdS/ZnS photocatalyst

In a typical synthesis, certain amount of as-prepared GO was dispersed in 30ml deionized water to obtain a homogeneous GO dispersion. After 15min ultrasonic treatment with agitating, 0.0416g Cadmium chloride (CdCl₂ · 2.5H₂O) and 0.0248g Zinc chloride (ZnCl₂) were introduced into the GO dispersion under magnetic stirring. Then, 0.1756g L-cysteine was added into the above solution. The above mixture

solution was sonicated for the additional 5 min, resulting in the formation of a black cream dispersion. The pH of mixture solution was adjusted to 7 by 1mol/L NaOH. Then, 0.0876g Sodium sulfide (Na_2S) was immersed into the mixture solution followed by magnetically stirring vigorously with the flowing N_2 for 15 min. The above mixture suspension was transferred into a 50 mL Teflon lined stainless steel autoclave and heated 180 °C for 1h in an oven. During this hydrothermal treatment, the reduction of GO can be simultaneously achieved²⁵. The autoclave was cooling down to the room temperature, the blackish green precipitate was collected by centrifugation and washed several times with deionized water or ethanol to remove possible remaining cations and anions. The obtained RGO-CdS/ZnS photocatalyst was dried in the vacuum oven for further characterization. The pure CdS/ZnS photocatalyst was prepared under the same condition without adding of GO.

2.3. Catalyst characterization

X-ray diffraction (XRD) technique was used to analysis the crystal structure of as-prepared photocatalyst. In this work, XRD patterns were obtained by a D/max-RA X-ray diffractometer (Rigaku, Japan) equipped with Ni-filtrated Cu Ka radiation (40 kV, 200 mA). The 2θ scanning angle range was 10–90° with a step of 0.02°/0.2 s. Raman experiments were performed using a DXR spectrometer using the 532 nm laser line, and measurements were made in backscattering geometry. X-ray photoelectron spectroscopy (XPS) data was recorded with a PHI5300 spectrometer using Al K (12.5 kV) X-ray source. The SEM images were examined with S-4800 scanning electron microscopy (HITACHI, Japan). Transmission electron microscopy

(TEM) and high resolution transmission electron microscopy (HRTEM) images were collected on an F20 S-TWIN electron microscope (Tecnai G2, FEI Co.), using a 200 kV accelerating voltage. Fourier transform infrared (FT-IR) spectra were recorded on a Nicolet Nexus 470 FT-IR (America thermo-electricity Company) with 2 cm^{-1} resolution in the range 400–4000 cm^{-1} , using KBr pellets. UV–vis diffuse reflectance spectra (UV–vis DRS) of photocatalyst powder was obtained for the dry-pressed disk samples using Specord 2450 spectrometer (Shimazu, Japan) equipped with the integrated sphere accessory for diffuse reflectance spectra, using BaSO_4 as the reference sample. Thermal gravimetry (TG) curves of samples were acquired by using a thermo-analysis instrument (NETZSCH STA 449C). Specific surface area of samples was measured (BET method) by nitrogen adsorption desorption isotherms using a NOVA 2000e analytical system (Quantachrome Co., USA). The photoluminescence (PL) spectra were obtained on a F4500 (Hitachi, Japan) photoluminescence detector.

2.4. Measurement of photocatalytic activity

The photocatalytic activity of RGO-CdS/ZnS photocatalyst was investigated by the degradation of TC under visible light irradiation. The photocatalytic reaction was carried out in the GHX-2 photocatalytic reactor with a 300W xenon lamp and a cutoff filter ($\lambda > 420$ nm) which can eliminate the effect of UV light. During the photocatalytic process, a circulating water jacket was conducted to keep the system temperature constant. In a typical process, 0.05g of photocatalyst was suspended into 100 mL TC (15mg/L) solution. After 30 min magnetic stirring in the dark, it reached

adsorption-desorption equilibrium, then initial absorbency (C_0) was determined. Prior to irradiation, 10 min interval of visible light irradiation sample was collected to measure the adsorption-desorption equilibrium. After visible light illumination, 8 mL of samples were taken out at a regular time interval (10 min) and separated through centrifugation (10000 rpm, 10 min). By the circulation of water, the temperature of the solution was maintained at about 298 K. Then, the UV-vis adsorption spectrum of the centrifuged solution was recorded using an UV-vis spectrophotometer. Finally, the degree of degradation is expressed by C/C_0 , which is the proportion of the temporal TC concentration to the TC concentration after adsorption process.

3. Results and discussion

3.1 Morphology and structure

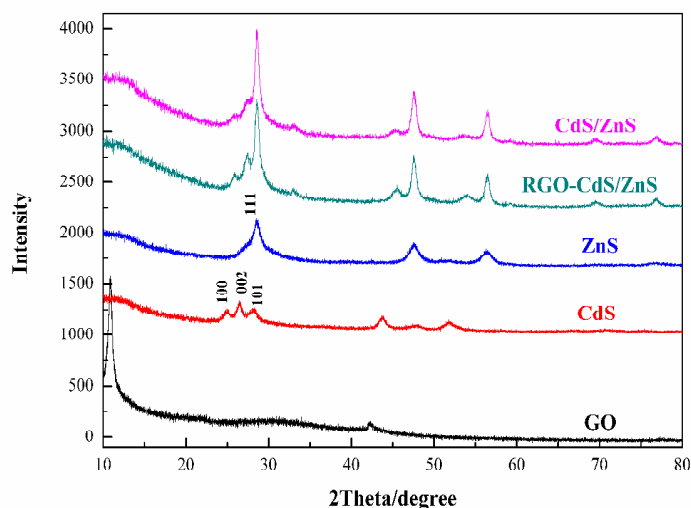


Fig. 1 XRD patterns of the GO, CdS, ZnS, CdS/ZnS and RGO-CdS/ZnS

XRD was used to determine the crystal structure and phase purity of the as-synthesized samples. The XRD patterns of GO, CdS, ZnS, CdS/ZnS and

RGO-CdS/ZnS photocatalysts are reflected in Fig.1. As the Fig. 1 shows, the XRD pattern of GO exhibits a sharply diffraction peak at $2\theta=11.004^\circ$, corresponding to an interlayer spacing of 0.87 nm larger than that of graphite (0.34 nm), which demonstrates the existence of oxygen-containing functional group such as hydroxyl and carboxyl groups³¹. Meanwhile, the diffraction peaks of CdS nanocrystal can be indexed to the cubic phase of CdS (JCPDS no. 41-1049), which is confirmed by the observed distinctive reflection peaks at $2\theta = 24.830^\circ, 26.646^\circ, 28.223^\circ, 44.021^\circ, 47.893^\circ$ and 52.153° . In addition, the diffraction peaks of ZnS at $2\theta= 28.822^\circ, 47.762^\circ$ and 56.355° can be indexed to the hexagonal zinc blend phase of ZnS (JCPDS no. 65-0309). Notably, it can be seen that the diffraction peaks of CdS/ZnS composites exhibited an obvious shift toward the higher angle compared with the pure CdS and ZnS. And the diffraction peak of (101) in CdS have been covered by the diffraction peak of (111) in ZnS. This indicates that Cd^{2+} have been incorporated into the lattice of the ZnS nanocrystal and increase the fringe lattice distance of the ZnS crystal due to the larger radius of Cd^{2+} ion (0.97 Å) which is higher than that of the Zn^{2+} ion (0.74 Å)³². Moreover, the crystallite size of CdS/ZnS heterostructure composites was calculated by the Scherrer formula³³. It can be found the particle size of CdS/ZnS is 13.22 nm which is corresponding to the TEM analysis. However, the diffraction peaks of RGO couldn't be observed from the XRD pattern of RGO-CdS/ZnS and the peak of CdS/ZnS have been weaken in the existence of RGO, which be attributed to the regular stack of RGO sheets have been reduced or destroyed by CdS/ZnS heterostructure composites³⁴.

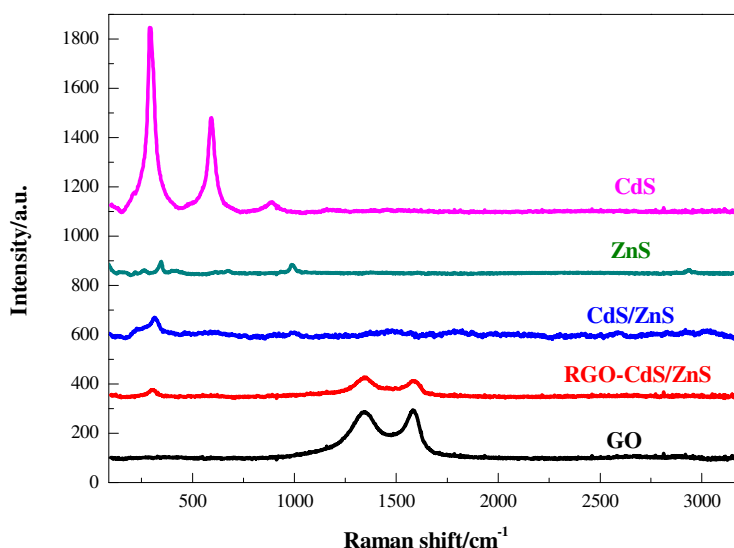


Fig.2 Raman spectra of GO, CdS, ZnS, CdS/ZnS and RGO-CdS/ZnS

Fig. 2 shows the Raman spectrum of RGO, CdS, ZnS, CdS/ZnS and RGO-CdS/ZnS heterostructure composites. Raman spectrum is also an effective method to investigate the true state of carbonaceous materials. Raman spectra of GO displays two significant peaks at ~ 1353 and ~ 1593 cm^{-1} , corresponding to the well-documented D band and G band, respectively³¹. The intensity ratio of D band to G band, namely the I_D/I_G ratio, shows the gauge for the amount of structural defects and a quantitative measure of edge plane exposure. For CdS nanocrystals, two characteristic peaks at 297.9 and 598.1 cm^{-1} were observed, corresponding to the 1st and 2nd longitudinal optical-phonon (LO) modes in CdS³⁵. Unlike the mode intensity of CdS nanocrystals, the peak of ZnS is dominated by the longitudinal optical (LO) phonon peak at 353 cm^{-1} , which is similar to report in the literature³⁶. However, the ragged Raman peak of CdS/ZnS at 297.9 cm^{-1} is clearly observed which could be demonstrated the existence of CdS. For CdS/ZnS, with the introduction of CdS, Cd^{2+}

have been incorporated into the lattice of the ZnS nanocrystal and increase the fringe lattice distance of the ZnS crystal due to the larger radius of Cd²⁺ ion (0.97 Å) which is higher than that of the Zn²⁺ ion (0.74 Å), thus the integrity crystal of CdS in CdS/ZnS have been broken³². Meanwhile, the surface defects and vacancies of ZnS increase the crystal defect of CdS/ZnS⁴⁵, thus resulting the disappearing of weak peak at 598.1 cm⁻¹ and the lower intensity peak at 297.9 cm⁻¹. For the spectral of RGO-CdS/ZnS, the I_D/I_G increase and a lower D band intensity is observed which could be attributed to the recovery of carbon atoms with defects in GO, indicating that the reestablishment of the conjugated RGO network³⁷. Compared with the CdS/ZnS, the Raman peak of CdS/ZnS in RGO-CdS/ZnS have been effected with the addition of GO which could be ascribed to the weak fluorescence properties of GO and the wavelength of raman exciting light, thus it shows the smaller intensity peak at 297.9cm⁻¹. In FTIR spectra, there is more evidence for the existence of the hydrophilic groups on the surface of graphene oxide. The picture of pure CdS/ZnS was shown as reference. In Fig. 3, the position of GO vibration bands are observed at 1057 cm⁻¹ (alkoxy C-O stretching), 1224 cm⁻¹ (phenolic C-OH stretching), 1402 cm⁻¹ (carboxyl O-H stretching), 1724 cm⁻¹ (C-O stretching vibrations of carboxyl or carbonyl groups), 3396 cm⁻¹ (hydroxyl groups or H₂O) and suggests that there are a lot of oxygen-containing hydrophilic groups in GO. After the hydrothermal treatment, the sample RGO-CdS/ZnS has a similar spectrum, but the peak at 1724 cm⁻¹ have been weaken and the sharply peak at 3449 cm⁻¹ have been moved to high wavelength which may be ascribed to the loss of oxygen groups and the reduction of GO after

hydrothermal treatment. According to the FTIR and Raman results, the CdS, ZnS and RGO have been chemically bonded.

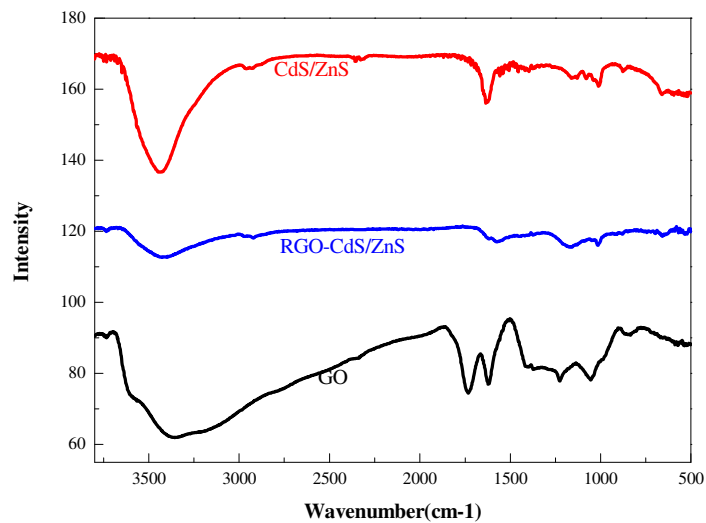


Fig. 3 FI-IR spectrum of GO, CdS/ZnS, RGO-CdS/ZnS

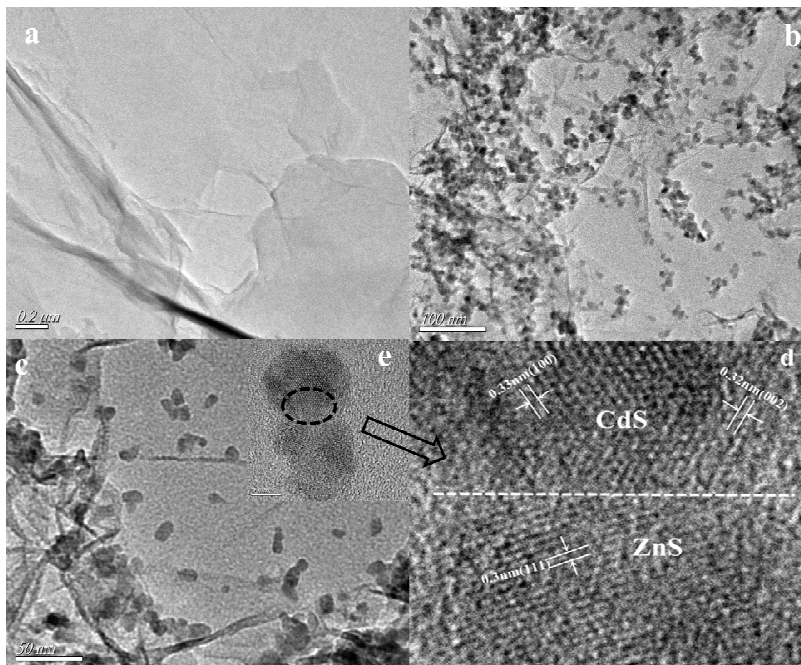


Fig.4 TEM image of GO (a), 15%RGO-CdS/ZnS(b,c), high-resolution TEM (HRTEM)

images of 15%RGO-CdS/ZnS(e)

The morphology and microstructure of sample was analyzed with TEM and high resolution TEM (HRTEM). As is shown in Fig. 4a, the blank-GO exhibits the sheet-like morphology with a smooth surface. The crumpled membrane indicates that GO sheets are flexible, and also GO sheets is multilayer rather than single layer which further confirms the results of sharply peak in XRD patterns of GO³⁸. In addition, the morphology of RGO-CdS/ZnS is evidently different from the solely GO. Fig. 4d shows that many CdS/ZnS nanoparticles have been assembled uniformly on the surface of RGO. Also, the uniform distribution of CdS/ZnS nanoparticles on RGO sheets can minimize the aggregation of nanoparticles and maximize the reactive sites which can enhance the photocatalytic performance. The TEM image (Fig. 4b) shows the diameter of CdS/ZnS around 13 nm which is corresponding to the value calculated by the Scherrer equation⁴⁹, showing that CdS/ZnS nanoparticles are exclusively deposited on the surface of RGO. Fig. 4(d,e) displays the HRTEM of CdS/ZnS nanoparticles. The measured lattice-fringe is 0.33, 0.32 and 0.3nm, indicated by the HRTEM, which agrees well with the spacing of (100), (002) and (111) lattice plane in CdS and ZnS. In Fig. 5, the distributions of Cd, Zn, C, O and S have been shown in the picture. There are no other impurities existing in the RGO-CdS/ZnS heterostructure composites.

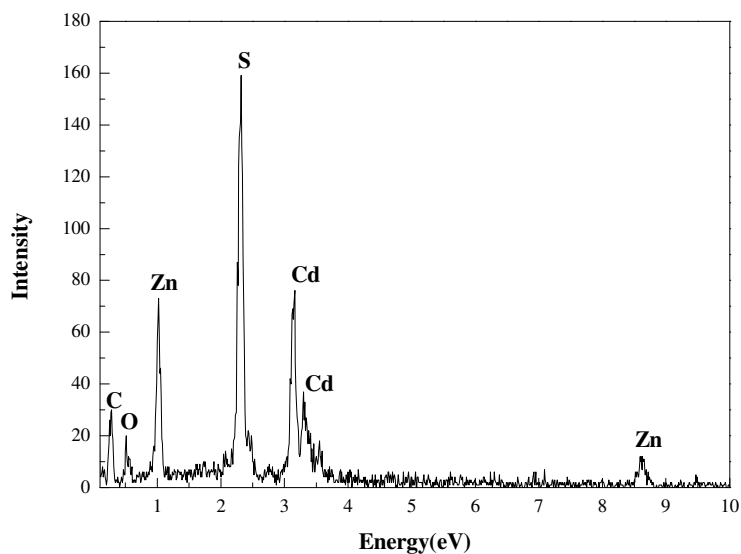


Fig. 5 EDX spectra of RGO-CdS/ZnS composites

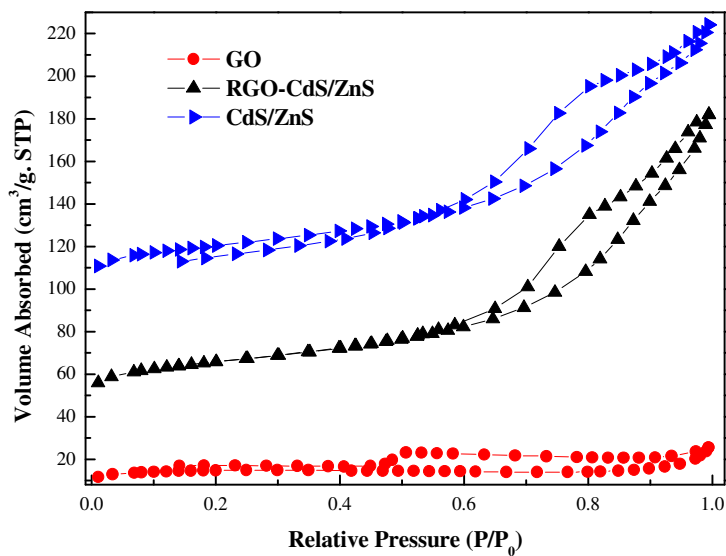


Fig. 6 The nitrogen adsorption–desorption isotherms of GO, CdS/ZnS and RGO-CdS/ZnS composites

The surface area of GO, CdS/ZnS and RGO-CdS/ZnS have also been investigated.

As displayed in Fig.6, the nitrogen adsorption–desorption isotherm of GO exhibits the

type IV isotherm with a hysteresis loop characteristic of type H2 according to the IUPAC classification, which indicates the presence of slit-shaped pores between parallel layers. The RGO-CdS/ZnS composite has an adsorption–desorption isotherm of type IV with a typical H3 hysteresis loop, which indicates the existence of slit-shaped pores between parallel layers and particle stacking. Therefore, the incorporation of RGO and CdS/ZnS has an obvious effect on the structure of the samples. The BET surface area of GO is measured to be ca. $50.5874 \text{ m}^2\text{g}^{-1}$, which is smaller than that of RGO-CdS/ZnS ($74.0057 \text{ m}^2\text{g}^{-1}$, respectively). Because of the BET surface of CdS/ZnS is too small, the nitrogen adsorption–desorption isotherm exhibit a type an II isotherm, indicating a nonporous structure according to the IUPAC classification³⁹. With the existence of RGO, the composites shows the higher BET surface and the tidy arrangement of microstructure.

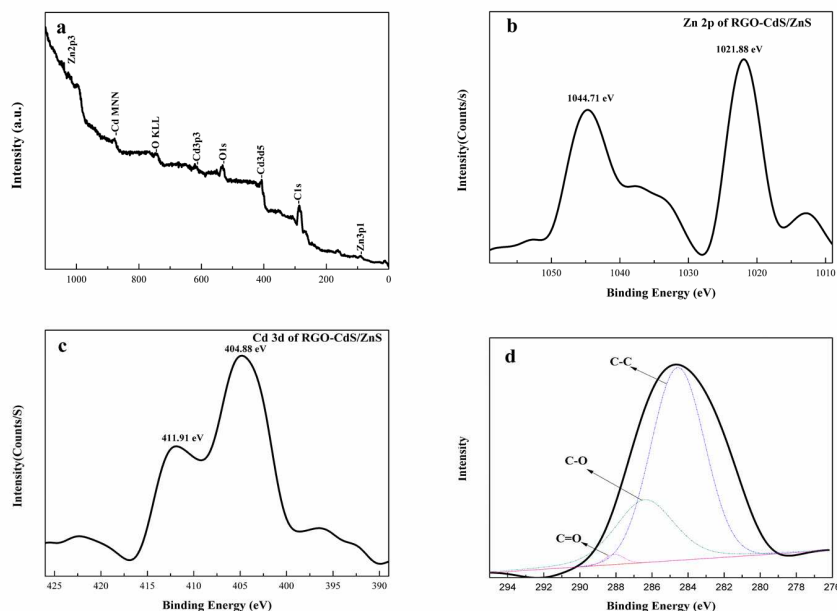


Fig.7 a) Full XPS spectra of RGO-CdS/ZnS composites, b) high resolution XPS spectrum of Zn 2p from RGO-CdS/ZnS composites, c) high resolution XPS spectrum

of Cd 2p from RGO-CdS/ZnS composites, d) high resolution XPS spectrum of C 1s from RGO-CdS/ZnS composites

In order to understand the bulk and chemical states of as-prepared photocatalysts, XPS analysis is explored to gain the deeper insight of composites photocatalysts. As the full XPS spectra of RGO-CdS/ZnS (Fig. 7) shows, all detected elements were C, O, Cd, Zn and S, which is consistent with the formation of RGO-CdS/ZnS composites and indicates the synthesis process doesn't bring any impurities deeply. Fig. 7d presented the high resolution XPS spectrum of C 1s from RGO-CdS/ZnS. The XPS peak of C1s was decomposed into four Gaussian peaks ranging from 275 to 295 eV. A strong peak centered at 284.63eV, corresponding to the C-C groups. In addition, the peak of C-O (286.4eV) and C=O (288.1eV) in the spectrum of C 1s can be assigned to the hydroxyl groups and carboxyl groups which confirms the characteristic peaks of GO⁴⁰. According to our previously work⁴¹, compared with the C 1s of RRGO-CdS/ZnS, the C1s of pure GO (Fig.S1(a)) displays the strong peak at 286.43eV which could be attributed to the stretching vibration of C-O groups. Also, the C-C shows the strongly intensity and other peak have been weakened in RRGO-CdS/ZnS, which suggests the partly removal of oxygen-containing groups. Two peaks have been observed for Cd 3d core levels at 404.81 eV and 411.91 eV which was deriving from a spin-orbit interaction with 3d³ (404.88eV) and 3d⁵ (411.91eV). What's more, the narrow and well-defined doublet characteristic peaks for the 3d structure indicates that cadmium is presented as Cd²⁺ in CdS. The high-resolution XPS spectra of Zn 2p is displayed in Fig. 7b. The binding energy of

1021.88eV corresponding to Zn 2p³ and the other peak at 1044.71 eV corresponding to Zn 2p¹. Both the binding energies of Cd 3d and Zn 2p is matched well with the report for the divalent zinc and cadmium in pure metal-sulphide³⁹.

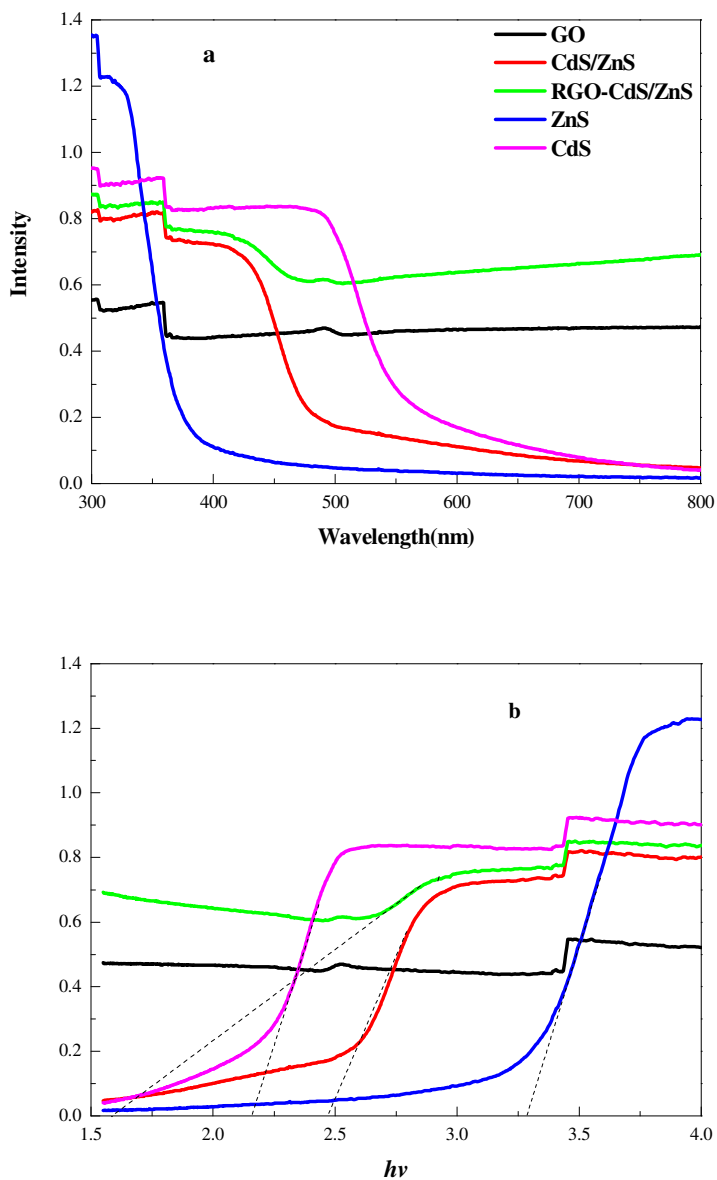


Fig.8 a) UV-vis absorption spectra of GO, CdS/ZnS, RGO-CdS/ZnS, ZnS, CdS b)

The plot of transformed Kubelka-Munk function versus the energy of light

What's more, the UV-vis diffuse reflectance spectra for the as-prepared samples

are displayed in Fig. 8a. Compared with the spectrum of pure ZnS, the adsorption spectrum of CdS/ZnS was transferred to the visible-light region. What's more, the RGO-CdS/ZnS exhibits the increased visible-light absorbance in comparison with other samples. A plot of the transformed Kubelka–Munk function of light energy $(\alpha hv)^2$ versus energy (hv) is also shown in Fig. 8b. From the Fig. 8b, the band gaps of the samples were estimated to be 2.49 eV, 2.18 eV, and 3.33 eV corresponding to CdS/ZnS, CdS and ZnS, respectively. The band gap of CdS/ZnS composites is 2.49eV which is bigger than CdS, while the following photocatalytic performance of CdS/ZnS composites is better than CdS. Thus could be attributed to the increasing photo-stability of photocataysts when ZnS was incorporated with CdS. Compared with the CdS/ZnS composites, the absorption edge of RGO-CdS/ZnS composites was red-shifted and the narrow band gap could be clearly observed. As the following Fig.8(b) shows, the band gaps of RGO-CdS/ZnS sample show about 1.52-1.55eV, which could be attributed to the chemical bonding between CdS/ZnS and the specific sites of carbon materials³⁸. With a red shift of RGO-CdS/ZnS in the absorbance demonstrates an decrease in the band gap than other samples, and the near-vertical adsorption edge shows the narrow size distribution and uniform crystallites. Furthermore, the RGO-CdS/ZnS composites shows the continuous absorbance in the visible range from 410 to 520 nm, which is RGO can enhance the surface electric charge of CdS/ZnS composites. Based on the continuous absorbance, RGO-CdS/ZnS composites are more efficient to utilize visible light.

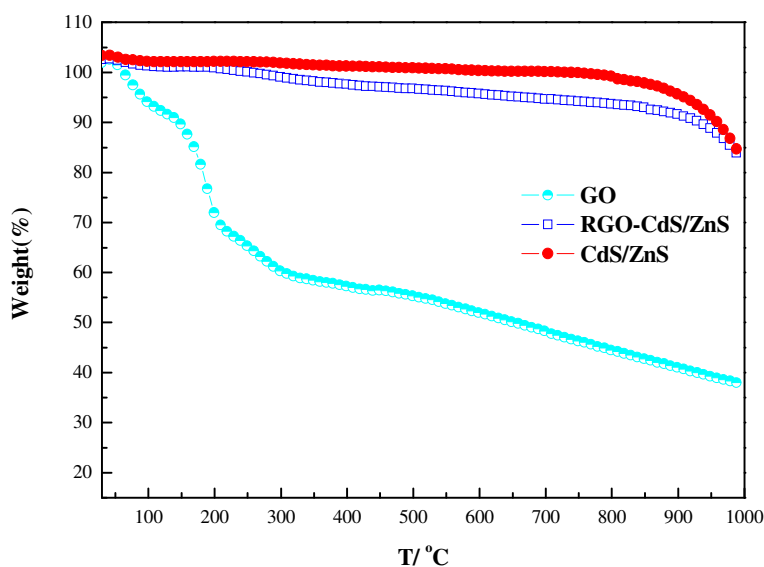


Fig. 9 TGA curves for GO, CdS/ZnS, RGO-CdS/ZnS

Thermogravimetric analysis (TGA) of the GO, RGO-CdS/ZnS, CdS/ZnS (Fig. 9) displays the mass change when the samples are exposed to the heat treatment. From the TGA curve of the RGO, two prominent major weight losses could be observed; the first sharp loss (28.89%) occurred at the range of 50 to 200 °C. And this could be attributed to the residual water and the dehydroxylation of structural groups in RGO⁴². The other sharp weight loss of 9.01% has been observed at the range of 200 to 500 °C, which mainly because of RGO have reached its deflagration point and the solid is decomposed to a carbon soot. Then, a steady mass loss (9%) occurred over the whole temperature range of 500 to 900 °C, which could be assigned to the removal of some stable oxygen functionalities⁴³. About 45% of weight have lost in the heat treatment. As for CdS/ZnS, when the temperature is lower than 100°C, the TGA curve of CdS/ZnS only shows the slightly weight loss which may be attributed to the thermal desorption of water. The second weight loss have happened after 300 °C, due to the

chemical transformation and physical change, such as the phase change of as-prepared sample or sample was broken up⁴⁴. However, the TGA curve of RGO-CdS/ZnS shows also two major weight losses. Also, the major loss could be attributed to the residual water and the dehydroxylation of structural groups in RGO, corresponding to the TGA of CdS/ZnS and demonstrating the existence of RGO. Compared with the other samples, only about 6.55% of RGO-CdS/ZnS composites have lost during the calcinations process, which confirming the thermal stability of RRGO-CdS/ZnS.

3.2 Photocatalytic Degradation Results and Analysis

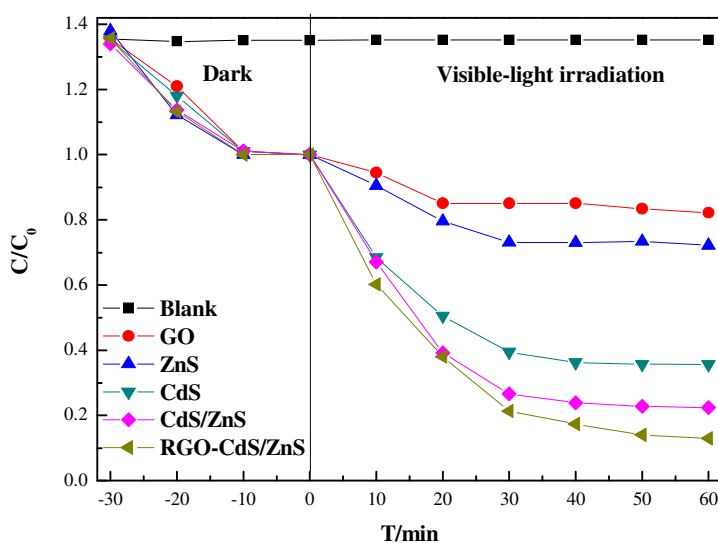


Fig.10 Photocatalytic behaviors of TC over GO, ZnS, CdS, CdS/ZnS and RGO-CdS/ZnS composites under visible light irradiation

The photocatalytic performance of samples was conducted by using the degradation of TC under the visible-light irradiation without adding any sacrificial reagents. ZnS, CdS, CdS/ZnS, GO and the blank solution were also investigated for the comparison. Fig. 10 shows the photocatalytic performance of GO, ZnS, CdS,

CdS/ZnS and RGO-CdS/ZnS. Before the light irradiation, the solution of TC and photocatalyst had been magnetically stirred in dark for 30 min to establish an adsorption-desorption equilibrium. Among them, the RGO-CdS/ZnS composites with the degradation rate (nearly 90%) have presented the first-rate photocatalytic performance in 60 min. It is clearly that ZnS and CdS have achieved the highest degradation rate at about 30min, which could be attributed to the photocorrosion of pure CdS and ZnS. Also, the CdS/ZnS exhibit the better photocatalytic activity than CdS and ZnS. What's more, the RGO-CdS/ZnS composites photocatalysts possess highest photodegradation rate than CdS/ZnS composites. The results may be caused by the existence of RGO which increase the surface area of CdS/ZnS. As the BET surface mentioned previously, the BET surface of RGO-CdS/ZnS is $74.0057 \text{ m}^2\text{g}^{-1}$ which is much larger than CdS/ZnS $30.13 \text{ m}^2\text{g}^{-1}$. With the higher surface area, the enhanced absorptivity which is mainly attributed to the electrostatic attraction between TC and aromatic regions of the graphene oxide, and more active sites are provided which result in higher photocatalytic efficiency. On the other hand, the appearing of the CdS/ZnS heterostructure and RGO which hindered the recombination process of electron-hole pairs. From the PL spectra (Fig. 13), the CdS displays the emission intensity peak centered at 535nm which could be attributed to the faster electron-hole pairs recombination rate, corresponding to the strongest PL signals. Because of the surface defects and vacancies, the ZnS displays the weak PL peak at 490nm⁴⁵. Compared with pure CdS and ZnS, the emission intensity of CdS/ZnS decrease means that the recombination of photogenerated electron-hole

pairs can be suppressed with the composition of CdS and ZnS. Also, it is found that a strong peak centered at 540 nm in CdS/ZnS, which corresponded to the green light region and a weak intensity peak for RGO-CdS/ZnS composites at 540 nm. It is well acknowledged that the recombination of photo-induced electron-hole pairs caused the PL emission intensity of semiconductor⁴⁶. Furthermore, upon light illumination, the photocurrent increases sharply reaching a steady state quickly. And, the current intensity returns quickly to the dark current state when the light is turned off. The presence of RGO leads to the enhancement of transient photocurrent response of CdS/ZnS from 14 mA cm⁻² to 25 mA cm⁻² for RGO-CdS/ZnS (Fig.14) composites, almost 3-5 times higher than that of the pure CdS and ZnS. Moreover, the transient photocurrents were rapid, steady and reproducible during several switched on-off cycles. As is known, the photocurrent is brought by the diffusion of free electron, which is directly direct correlation to the recombination efficiency of the photogenerated carriers⁴⁷. With the addition of RGO, the RGO-CdS/ZnS heterostructure photocatalysts have lower recombination of electron-hole pairs than CdS/ZnS, which promotes the more effectively migration of charge-carriers and the photocatalytic activity.

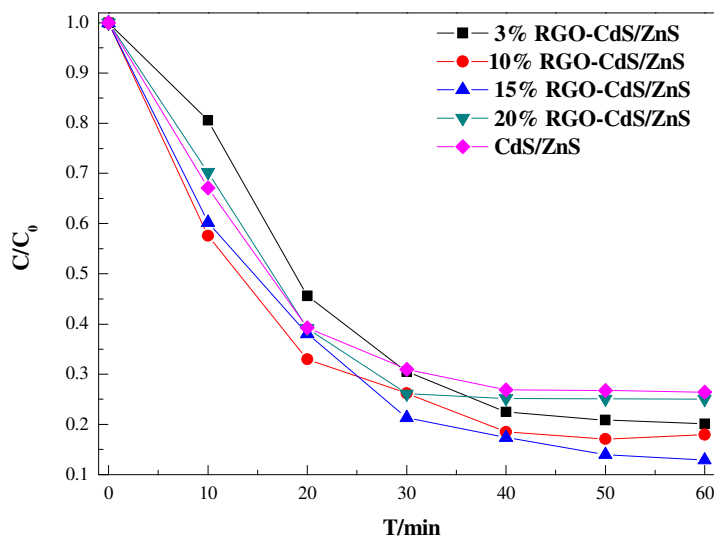


Fig. 11 Photodegradation behaviors of TC in presence of RGO-CdS/ZnS composites with different contents of RGO

Fig. 11 depicts the photocatalytic activity of photocatalysts with various content of RGO under visible light irradiation. Except the 15% RGO-CdS/ZnS, 3%, 10% and 20% RGO-CdS/ZnS have been synthesized in this experiment. With the RGO content increasing, the photodegradation rate is increasing firstly. The optimum amount of RGO is 15%, which shows the best photodegradation rate of TC. 15% RGO-CdS/ZnS shows the highest degradation rate about 88% with 60 min among the other RGO-CdS/ZnS composites. However, the degradation rate of 20% RGO-CdS/ZnS is lower than 3%, 10% and 15% RGO-CdS/ZnS, the reason could be attributed to superfluous RGO. Thus could increase the opacity and light scattering, then the light absorption decreasing which weaken the light intensity to the surface of photocatalysts, just as is found in report⁴⁸. The results demonstrates that the suitable amount of RGO is a crucial factor in photocatalytic activity. What's more, the recycled run for the

photocatalytic experiment have been shown in Fig. 15. After every 60 min of photodegradation, the separated photocatalysts were washed with distilled water and dried. After four runs of the photodegradation of TC, the photocatalytic activity of 15% RGO-CdS/ZnS displays a slightly decrease, which demonstrates the RGO-CdS/ZnS is photo-stable while the pure CdS is easily photocorrosion in the photocatalytic process.

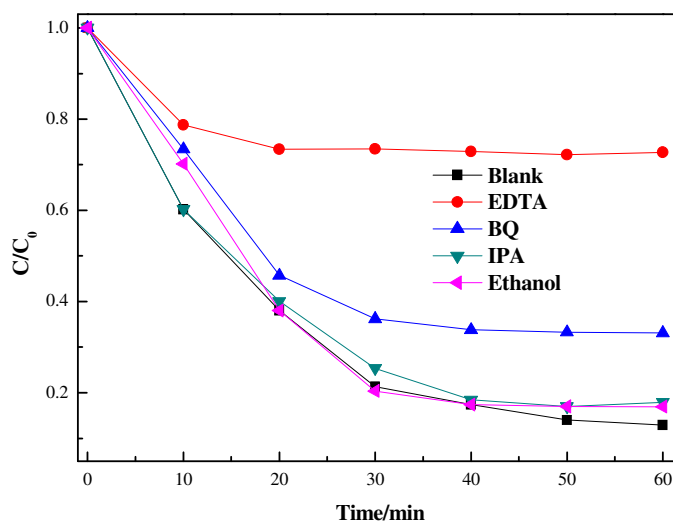


Fig. 12 Reactive species trapping experiments of RGO-CdS/ZnS composites

Furthermore, reactive oxidative species trapping experiments were performed to investigate the main oxidative species during the photocatalytic process by using different scavengers⁴⁹, *p*-benzoquinone (BQ, $O_2^{\bullet-}$ radicals scavenger), disodium ethylenediaminetetraacetate (EDTA, holes scavenger), ethanol (electron scavenger) and isopropanol (IPA, OH^{\bullet} radicals scavenger). The photodegradation of TC were significantly suppressed by the introduction of EDTA anions, indicating that holes are the main reactive oxidative species involved in the photocatalysis. In contrast, the

adding of BQ, Ethanol or IPA in the solution has no remarkably effect on the photocatalytic activity of RGO-CdS/ZnS, implying that electron and OH^\bullet radicals have no contribution for the degradation process. Moreover, the introduction of BQ into the photocatalytic system could also decrease the photocatalytic degradation of TC from 85% to about 68%, suggesting $\text{O}_2^{\bullet-}$ have a little effect on the degradation of TC.

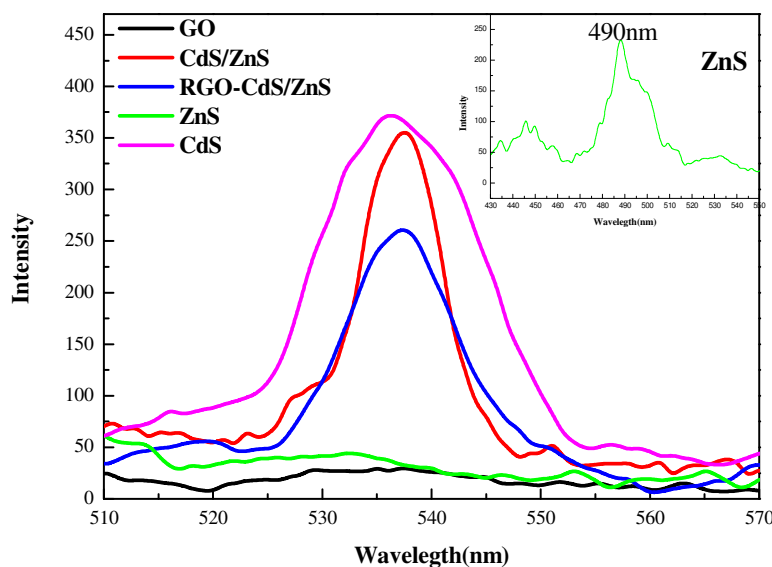


Fig. 13 PL spectra of sample GO, CdS/ZnS and RGO-CdS/ZnS at an excitation wavelength of 275 nm

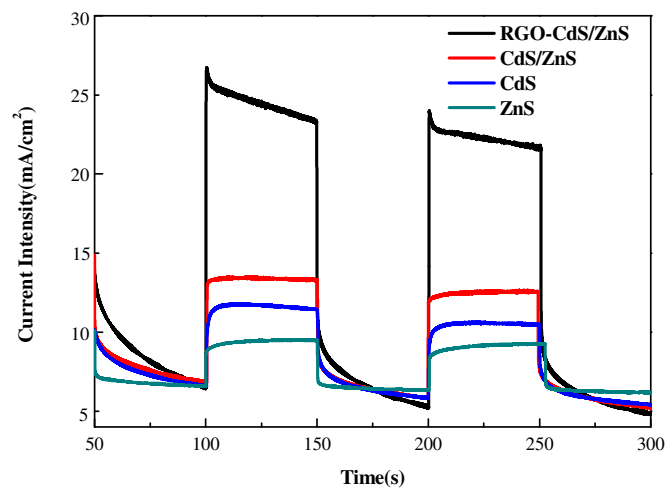


Fig 14 Photocurrent versus time (I-t) curves of the solar cell device based on CdS, ZnS, CdS/ZnS and RGO-CdS/ZnS composite in 0.2 M Na_2SO_4 aqueous solution under visible light irradiation with applied potential of 0.5 V vs Ag/AgCl.

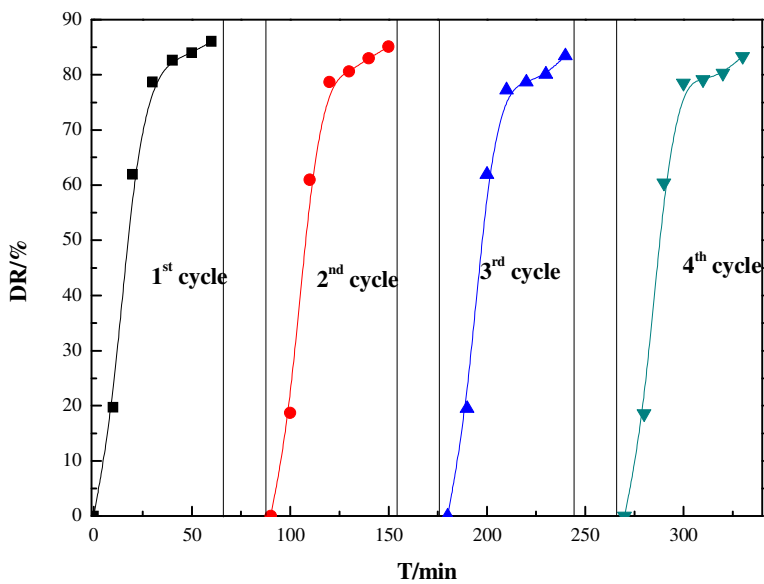


Fig.15 Repeated photocatalytic experiments of RGO-CdS/ZnS composites

3.3 Photocatalytic Mechanism

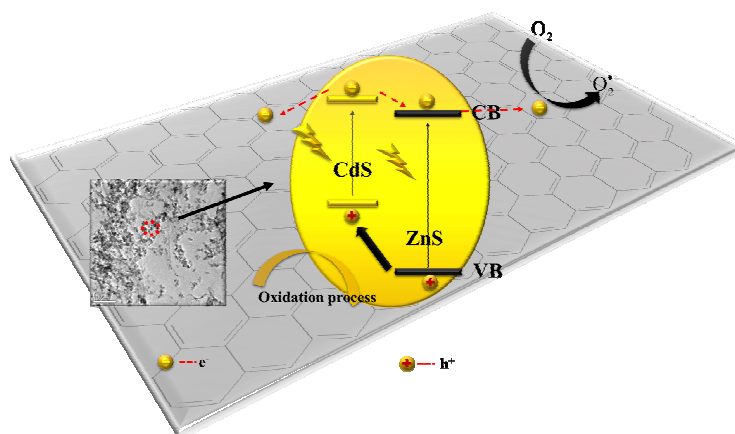


Fig.16 Energy band diagram and photogenerated electron–hole pairs transfer of photocatalysts

Based on the results described above, we have proposed the following possible mechanism. As is shown in Fig. 16, a schematic illustration of the charge transfer and photocatalytic activity by RGO-CdS/ZnS composites is summarized. Under visible light irradiation, the electron–hole pairs in CdS are firstly excited, and the electrons are excited to the conduction band (CB), inducing the formation of holes in the VB. The potential of ZnS is about -0.91eV , which is less negative than the CB level of CdS (about -0.95 V), the electrons in the CB of CdS could be transferred into the CB of ZnS directly which is driven by the band potential. And also, the free photo-generated electrons in the CB of ZnS can be captured by RGO, which is attributed to the two-dimensional carbon network. So the photo-generated electrons of ZnS and RGO were so lively to take part in the surface reaction to form radicals, thus dramatically producing the visible-light activity⁵⁰. The novel electron transfer channel results in the efficient separation of photo-generated electron-hole pairs and the photo-generated electrons can be captured by adsorbed oxygen molecules, leading to the generation of

hydrogen peroxide or superoxide radical ($O_2^{\bullet-}$) which is also a powerful oxidative specie for TC degradation. Meanwhile, the photogenerated holes could be transferred to the valence band (VB) of CdS from the ZnS. In this way, the photogenerated holes in the VB of CdS can directly oxidize TC to harmless products. However, compared to the $\bullet OH/H_2O$ potential (ca. 2.27 V), the VB levels of RGO-CdS/ZnS is not positive enough to drive the oxidation process of H_2O to form $\bullet OH$ due to the insufficient oxidation ability, which is also confirmed by the photoluminescence technique using coumarin as a probe molecule to detect $OH\bullet$ ⁵¹. The results displayed that few $OH\bullet$ could be found in the photocatalytic process here. This explains clearly why $OH\bullet$ has a little effect on the photocatalytic activity. In the recently published reports⁵², the role of RGO and some other electron transport materials, such as conducting graphite also have been reported to reduce the recombination rate of electron-hole species in the semiconductors under light irradiation. In this view of point, the higher BET surface area and strong adsorption ability for TC antibiotics of RGO, the relative narrower band-gap of CdS/ZnS composites as well as the increasing absorbance in the visible light region compared with pure ZnS, the lower recombination rate of the photoexcited electrons and holes prolong the lifetime of photogenerated carrier, thus greatly improve the photocatalytic activity and stability of RGO-CdS/ZnS composites in the removal of pollutants.

4. Conclusion

In this paper, by loading reduced graphene oxide as the electron transport materials, we have developed a novel hydrothermal method to synthesis the ternary

reduced graphene oxide-CdS/ZnS heterostructures as a photocatalyst for purifying water under the visible-light irradiation. The CdS/ZnS heterostructure and reduced graphene oxide have played an important role on degradation of Tetracycline under visible light irradiation. Owing to the CdS/ZnS heterostructures, CdS/ZnS not only shows the better photocatalytic activity but also the CdS/ZnS heterostructure prevent pure CdS or ZnS from photocorrosion. The as-prepared reduced graphene oxide-CdS/ZnS have been demonstrated to highly active in photodegradation of Tetracycline (about 85%) and the highest degradation ratio was found in sample with the content of 15% reduced graphene oxide. Also, reduced graphene oxide-CdS/ZnS shows the remarkable photocatalytic activity for the stability and cyclic performances. The present study provides a guidance to design and fabricate novel photoactive materials for catalysis and other applications.

Acknowledgements

This work was financially supported by the Natural Science Foundation of China (No.21207053), the Natural Science Foundation of Jiangsu Province (No.BK20131259, BK20130489, BK20140532), the program for Postgraduate Research Innovation in University of Jiangsu Province (No.KYLX1028) and the Research Foundation of Jiangsu University, China (No.11JDG107).

Reference

1. S. Ahmed, M. Rasul, W. N. Martens, R. Brown and M. Hashib, *Water, Air, & Soil Pollution*, 2011, **215**, 3-29.
2. M. N. Chong, B. Jin, C. W. Chow and C. Saint, *Water research*, 2010, **44**,

- 2997-3027.
3. Z. Liu, W. Hou, P. Pavaskar, M. Aykol and S. B. Cronin, *Nano letters*, 2011, **11**, 1111-1116.
 4. Y. Min, K. Zhang, W. Zhao, F. Zheng, Y. Chen and Y. Zhang, *Chemical Engineering Journal*, 2012, **193-194**, 203-210.
 5. Y. P. Xie, G. Liu, L. Yin and H. M. Cheng, *Journal of Materials Chemistry*, 2012, **22**, 6746-6751.
 6. J. Kim, C. W. Lee and W. Choi, *Environmental science & technology*, 2010, **44**, 6849-6854.
 7. O. Akhavan, *Acs Nano*, 2010, **4**, 4174-4180.
 8. A. P. Davis and C. Huang, *Water Research*, 1991, **25**, 1273-1278.
 9. M. Sathish and R. P. Viswanath, *Catalysis Today*, 2007, **129**, 421-427.
 10. V. M. Dzhagan, M. Y. Valakh, C. Himcinschi, A. G. Milekhin, D. Solonenko, N. A. Yeryukov, O. E. Raevskaya, O. L. Stroyuk and D. R. T. Zahn, *The Journal of Physical Chemistry C*, 2014, **118**, 19492-19497.
 11. B. Weng, S. Q. Liu, N. Zhang, Z. R. Tang and Y. J. Xua, *Journal of Catalysis*, 2014, **309**, 146-155.
 12. Muhammad Arshad Kamran, R. B. Liu, L. J. Shi, B. Zou and Q. L. Zhang, *The Journal of Physical Chemistry C*, 2013, **117**, 17777--17785.
 13. H. G. Cha, H. S. Noh, M. J. Kang and Y. S. Kang, *New Journal of Chemistry*, 2013, **37**, 4004-4009.
 14. S. Zhang, Q. Y. Chen, D. W. Jing, Y. H. Wang and L. J. Guo, *International*

- journal of hydrogen energy*, 2012, **37**, 791-796.
15. M. A. Hossain, J. R. Jennings, Z. Y. Koh and Q. Wang, *ACS nano*, 2011, **5**, 3172-3181.
 16. D. Chronopoulos, N. Karousis, S. Zhao, Q. Wang, H. Shinohara and N. Tagmatarchis, *Dalton Transactions*, 2014, **43**, 7429-7434.
 17. M. Q. Yang, N. Zhang, M. Pagliaro and Y. J. Xu, *Chemical Society Reviews*, 2014, **43**, 8240-8254.
 18. N. Zhang, Y. H. Zhang and Y. J. Xu, *Nanoscale*, 2012, **4**, 5792-5813.
 19. X. W. Wang, G. Liu, Z. G. Chen, F. Li, G. Q. Lu and H. M. Cheng, *Journal of Materials Research*, 2010, **25**, 39.
 20. B. T. Liu, W. J. Xu, T. Sun, M. Chen, L. L. Tian and J. B. Wang, *New Journal of Chemistry*, 2014, **38**, 2273-2277.
 21. A. Deshpande, P. Shah, R. Gholap and N. M. Gupta, *Journal of colloid and interface science*, 2009, **333**, 263-268.
 22. J. Zhang, J. Yu, M. Jaroniec and J. R. Gong, *Nano letters*, 2012, **12**, 4584-4589.
 23. Y. X. Yin, Z. G. Jin and F. Hou, *Nanotechnology*, 2007, **18**, 495608.
 24. X. W. Wang, G. Liu, Z. G. Chen, F. Li, L. Z. Wang, G. Q. Lu and H. M. Cheng, *Chemical Communications*, 2009, 3452-3454.
 25. C. Han, Z. Chen, N. Zhang, J. C. Colmenares and Y. J. Xu, *Advanced Functional Materials*, 2015, **25**, 221-229.
 26. N. Zhang, M. Q. Yang, Z. R. Tang and Y. J. Xu, *ACS Nano*, 2014, **8**, 623-633.

27. Q. Li, B. Guo, J. Yu, J. Ran, B. Zhang, H. Yan and J. R. Gong, *Journal of the American Chemical Society*, 2011, **133**, 10878-10884.
28. A. N. Cao, Z. Liu, S. S. Chu, M. H. Wu, Z. M. Ye, Z. W. Cai, Y. L. Chang, S. F. Wang, Q. H. Gong and Y. F. Liu, *Advanced Materials*, 2010, **22**, 103-106.
29. F. Liu, X. Shao, J. Wang, S. Yang, H. Li, X. Meng, X. Liu and M. Wang, *Journal of Alloys and Compounds*, 2013, **551**, 327-332.
30. R. A. Figueroa, A. Leonard and A. A. MacKay, *Environmental science & technology*, 2004, **38**, 476-483.
31. D. C. Marcano, D. V. Kosynkin, J. M. Berlin, A. Sinitskii, Z. Sun, A. Slesarev, L. B. Alemany, W. Lu and J. M. Tour, *ACS nano*, 2010, **4**, 4806-4814.
32. Q. Li, H. Meng, P. Zhou, Y. Q. Zheng, J. Wang, J. G. Yu and J. R. Gong, *ACS Catalysis*, 2013, **3**, 882-889.
33. W. N. Xing, L. Ni, P. W. Huo, Z. Y. Lu, X. L. Liu, Y. Y. Luo and Y. S. Yan, *Applied Surface Science*, 2012, **259**, 698-704.
34. P. Gao, J. C. Liu, D. D. Sun and W. Ng, *Journal of hazardous materials*, 2013, **250-251**, 412-420.
35. R. Rossetti, S. Nakahara and L. Brus, *The Journal of Chemical Physics*, 1983, **79**, 1086-1088.
36. O. Brafman and S. Mitra, *Physical Review*, 1968, **171**, 931.
37. S. Linley, Y. Y. Liu, C. J. Ptacek, D. W. Blowes and F. X. Gu, *ACS applied materials & interfaces*, 2014, **6**, 4658-4668.
38. Y. H. Zhang, Z. R. Tang, X. Z. Fu and Y. J. Xu, *ACS Nano*, 2010, **4**,

- 7303-7314.
39. N. Zhang, M. Q. Yang, Z. R. Tang and Y. J. Xua, *Journal of Catalysis*, 2013, **303**, 60-69.
40. S. G. Pan and X. H. Liu, *Journal of Solid State Chemistry*, 2012, **191**, 51-56.
41. M. J. Zhou, D. L. Han, X. L. Liu, C. C. Ma, H. Q. Wang, Y. F. Tang, P. W. Huo, W. D. Shi, Y. S. Yan and J. H. Yang, *Applied Catalysis B: Environmental*, 2015, **172-173**, 174-184.
42. S. Luo, X. Xu, G. Zhou, C. Liu, Y. Tang and Y. Liu, *Journal of hazardous materials*, 2014, **274**, 145- 155.
43. M. Z. Kassae, E. Motamedi and M. Majdi, *Chemical Engineering Journal*, 2011, **172**, 540-549.
44. H. Sekhar and D. N. Rao, *Journal of Physical Chemistry C*, 2013, **117**, 2300-2307.
45. M. Sookhakian, Y. M. Amin, R. Zakaria, W. J. Basirun, M. R. Mahmoudian, B. Nasiri-Tabrizi, S. Baradaran and M. Azarang, *Journal of Alloys and Compounds*, 2015, **632**, 201-207.
46. N. Biswal and K. M. Parida, *International journal of Hydrogen Energy*, 2013, **38**, 1267- 1277.
47. W. J. Han, L. Ren, X. Qi, Y. D. Liu, X. L. Wei, Z. Y. Huang and J. X. Zhong, *Applied Surface Science*, 2014, **299**, 12-18.
48. B. Chai, J. Li and Q. Xu, *Industrial & Engineering Chemistry Research*, 2014, **53**, 8744-8752.

49. C. Han, M. Q. Yang, N. Zhang and Y. J. Xu, *Journal of Materials Chemistry A*, 2014, **2**, 19156-19166.
50. C. Cui, Y. P. Wang, D. y. Liang, W. Cui, H. H. Hu, B. q. Lu, S. Xu, X. Y. Li, C. Wang and Y. Yang, *Applied Catalysis B: Environmental*, 2014, **158-159**, 150-160.
51. D. F. Xu, B. Cheng, S. W. Cao and J. G. Yu, *Applied Catalysis B: Environmental*, 2015, **164**, 380-388.
52. Y. H. Zhang, N. Zhang, Z. R. Tang and Y. J. Xu, *ACS nano*, 2012, **6**, 9777-9789.